Molecular Therapy
Methods & Clinical Development
Original Article

Safety of Same-Eye Subretinal Sequential Readministration of *AAV2-hRPE65v2* in Non-human Primates

Lindsey Weed,[1] Michael J. Ammar,[1] Shangzhen Zhou,[1] Zhangyong Wei,[1] Leona W. Serrano,[1] Junwei Sun,[1] Vivian Lee,[1,2] Albert M. Maguire,[1,2] Jean Bennett,[1,3] and Tomas S. Aleman[1,3]

[1]Center for Advanced Retinal and Ocular Therapeutics (CAROT), Department of Ophthalmology, University of Pennsylvania Perelman School of Medicine, Philadelphia, PA, USA; [2]Department of Dermatology, University of Pennsylvania Perelman School of Medicine, Philadelphia, PA, USA; [3]The Children's Hospital of Philadelphia (CHOP), Philadelphia, PA, USA

We have demonstrated safe and effective subretinal readministration of recombinant adeno-associated virus serotype (rAAV) to the contralateral eye in large animals and humans even in the setting of preexisting neutralizing antibodies (NAbs). Readministration of AAV to the same retina may be desirable in order to treat additional areas of the retina not targeted initially or to boost transgene expression levels at a later time point. To better understand the immune and structural consequences of subretinal rAAV readministration to the same eye, we administered bilateral subretinal injections of rAAV2-*hRPE65v2* to three unaffected non-human primates (NHPs) and repeated the injections in those same eyes 2 months later. Ophthalmic exams and retinal imaging were performed after the first and second injections. Peripheral blood monocytes, serum, and intraocular fluids were collected at baseline and post-injection time points to characterize the cellular and humoral immune responses. Histopathologic and immunohistochemical studies were carried out on the treated retinas. Ipsilateral readministration of AAV2-*hRPE65v2* in NHPs did not threaten the ocular or systemic health through the time span of the study. The repeat injections were immunologically and structurally well tolerated, even in the setting of preexisting serum NAbs. Localized structural abnormalities confined to the outer retina and retinal pigmented epithelium (RPE) after readministration of the treatment do not differ from those observed after single or contralateral administration of an AAV carrying a non-therapeutic transgene in NHPs and were not observed in a patient treated with the nearly identical, FDA-approved, AAV2-*hRPE65v2* vector (voretigene neparvovec-rzyl), suggesting NHP-specific abnormalities.

INTRODUCTION

Inherited retinal dystrophies (IRDs) are a large group of molecularly and clinically heterogeneous conditions caused by mutations in genes expressed in the neural retina and retinal pigmented epithelium (RPE). To date, mutations in over 270 genes have been reported to cause various IRDs ranging in severity from a mild, gradual, late onset of vision loss to blindness soon after birth.[1–3] Until very recently, there was no available treatment for IRDs. The US Food and Drug Administration (FDA) and the European Medicines Agency (EMA) recently approved AAV2-*hRPE65v2* (voretigene neparvovec-rzyl, Luxturna, Spark Therapeutics, Philadelphia, PA, USA) for subretinal delivery as gene augmentation treatment for an early onset, autosomal recessive IRD caused by bi-allelic *RPE65* mutations. RPE65 is an isomerohydrolase expressed in the RPE that mediates the conversion of all-trans retinyl ester to 11-*cis* retinol, a key component of light-absorbing pigments in photoreceptor cells.[4–6] Mutations in *RPE65* disrupt the visual cycle and cause early onset IRD known as Leber's congenital amaurosis (LCA).[7–9] Voretigene neparvovec-rzyl, the name for the clinical-grade version of AAV2-*hRPE65v2*, carries the wild-type version of the human *RPE65* cDNA driven by a constitutive chicken β-actin with a cytomegalovirus enhancer promoter packaged in recombinant adeno-associated virus serotype 2 (rAAV2). This is delivered to the tissue by subretinal injection.[10–12]

The subretinal injections typically lead to transduction of retinal cells only within the area of the localized transient retinal detachment or "bleb" that result.[13] Thus, visual improvement, although impressive, is limited to the location and extent of the treated region. Ipsilateral readministration of gene therapy agents to the retina could be useful in several situations. A likely scenario would be the need to treat additional areas of the retina not targeted during the initial injection, because the blebs do not predictably track to the region planned for treatment pre-operatively. In other scenarios, fragile regions such as the fovea may have been deliberatively spared over concerns of potential tissue damage and potential central vision loss. In such scenarios,

Received 7 July 2019; accepted 26 August 2019;
https://doi.org/10.1016/j.omtm.2019.08.011.

Correspondence: Jean Bennett, Center for Advanced Retinal and Ocular Therapeutics (CAROT), Department of Ophthalmology, University of Pennsylvania Perelman School of Medicine, Philadelphia, PA, USA.
E-mail: jebennet@pennmedicine.upenn.edu
Correspondence: Tomas S. Aleman, Center for Advanced Retinal and Ocular Therapeutics (CAROT), Department of Ophthalmology, University of Pennsylvania Perelman School of Medicine, Philadelphia, PA, USA.
E-mail: aleman@pennmedicine.upenn.edu

Table 1. Summary of Characteristics of Animals Used in the Study

				Injection #1				Injection #2				Readmin. Bleb Locations[a]
				Right Eye		Left Eye		Right Eye		Left Eye		
Animal ID	Species	Gender	Age (Years)	Volume (μL)	Dose [vg × 10^{11}]	Volume (μL)	Dose (vg × 10^{11})	Volume (μL)	Dose (vg × 10^{11})	Volume (μL)	Dose (vg × 10^{11})	
10C015	cynomolgus (*Macaca fascicularis*)	F	8	180	1.8	120	1.2	200	2.0	150	1.5	no overlap
BF54F	rhesus (*Macaca mulatta*)	M	9	100	1.0	150	1.5	150	1.5	150	1.5	partial overlap
11D086	cynomolgus (*Macaca fascicularis*)	F	7	180	1.8	120	1.2	200	2.0	200	2.0	complete overlap

Age is given for the first injection time point. vg, vector genomes.
[a]Relative position of the readministered (readmin.) subretinal bleb in relationship to initial bleb that resulted from the first injection.

it may be desirable to treat the fovea and/or previously untreated regions at a later time point. Finally, if transgene expression levels were to subside over time after a single injection, readministration could be used as a booster in previously transduced cells.[14,15]

The immune and ocular inflammatory response after the subretinal administration of AAV2-*hRPE65* in pre-clinical studies in dogs and non-human primate (NHPs) defined the dose range for safe delivery of the vector to patients.[13,16–18] Subretinal delivery of gene therapy agents has proven effective and relatively benign, in large part due to the fact that the retina is an immunologically privileged site.[19–21] We further demonstrated that subretinal readministration of AAV2-*hRPE65v2* to the contralateral eye is well tolerated, does not elicit an inflammatory immune response, and results in the predicted gain in retinal function both in affected dogs and in patients.[22–25] However, to our knowledge, there are no reports of repeated delivery into an already injected retina. The main concern is that local disruption of physical barriers during the initial intervention may prime the immune system to mount a potentially harmful immune response upon readministration of the vector to the same eye.[26,27] Therefore, a comprehensive understanding of ocular immunogenicity to AAV vectors upon same eye readministration will be useful in defining the safety and feasibility of this procedure.

NHP (macaque) eyes are close in size and have similar anatomical constituents and proportions compared to human eyes, including the existence of a nearly identical macular region.[28–30] Despite expected immunologic differences between humans and NHPs, the ocular immune response to AAV vector administration in NHPs has proven a good predictor of the human immune response.[24,31–33] To determine the humoral and cellular immune response to same eye subretinal readministration, we performed studies using GMP-comparable rAAV2-*hRPE65v2* (nearly identical to voretigene neparvovec-rzyl) in healthy NHPs. We carried out serial *in vivo* multimodal retinal imaging after sequential subretinal administration of the vector to the same eye in order to assess changes over time that might correlate with the systemic and local immunologic profile and histopathologic changes *ex vivo*.

RESULTS

Effects of Bilateral Same-Eye Subretinal Readministration of AAV2-*hRPE65v2* in NHPs

Evaluated were three unaffected NHPs ~7 to 8 years old at the start of the study (Table 1). Two were cynomolgus and one was a rhesus macaque. All animals had been studied previously in a pharmacology study that did not involve the eye, and their geographic origins were unknown. There was a >1 year washout between prior drug delivery and the AAV delivery that took place in the current study. Subretinal injections of AAV2-*hRPE65v2* were carried out bilaterally and animals were followed 3.5 months after the initial injections (Figure 1; Table 1). As expected based on our previous studies, the retinal detachments had resolved by the first ophthalmoscopy post-injection time point (3 days).[13,24] There were no cells in the anterior chamber (AC) or vitreous compartments. Pigmentary changes delineating the borders of the detachments ("blebs") were noted. Two months later, a second injection of similar volume and dose of AAV2-*hRPE65v2* was delivered subretinally in a region that overlapped either completely or partially or avoided altogether the initial treatment region in order to observe any differing effects between the three scenarios (Figure 1; Table 1). Retinal imaging was performed 43 and 65 days from the first and second injection, respectively (Figure 1). Visible "watermarks" demarcating the boundaries of the first bleb and vasculature landmarks served as landmarks for the readministration procedures. Pigmentary changes were present in the regions of injection, with hyperpigmentation at the borders of the injected region and hypopigmentation within the bleb in all eyes (Figure 2A). The changes are visible by ophthalmoscopy and have been observed as early as 3 days after the subretinal injections (data not shown). Fibrous metaplasia was also noted in the inferior blebs of both eyes of 10C015. The blebs were located at a similar distance relative to the optic nerve in superior and/or inferior retina, although some blebs extended into the central macula (Figure 1). The retina surrounding the blebs appeared normal (Figure 2A). *En face* retinal imaging with short

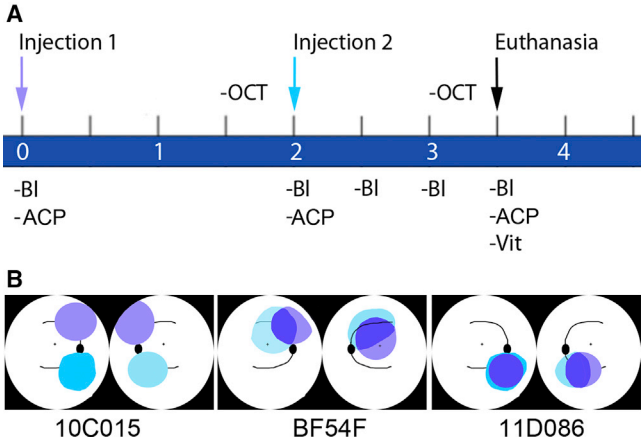

Figure 1. Experimental Design

(A) Timeline (in months) of injection procedures, sample collection, and in-life assays. Baseline samples were collected on day "0," immediately prior to the first subretinal injection. Similarly, samples were collected again immediately prior to the second subretinal injection on day 60. Blood samples were then collected every 2 weeks until termination of the study. Bl, phlebotomy; ACP, anterior chamber paracentesis; OCT, optical coherence tomography; Vit, vitreous biopsy. (B) Cartoons depicting the location and extent of the blebs created after the bilateral subretinal injections in each of the three animals for the first (violet) and second (turquoise) administrations for each eye. Regions of overlap of the two injections appear in blue. Right eye is the leftward-most image of each pair of cartoons per animal (i.e., cartoons are depicted as if one were looking into the animal's eyes).

wavelength fundus autofluorescence (SW-FAF) serves to monitor the health of the RPE, and indirectly the photoreceptors, by capturing the returning autofluorescence (AF) signal produced by the excitation by blue light of lipofuscin and melano-lipofuscin fluorophores within RPE cells.[34,35] After the initial injections, SW-FAF clearly delineates the edge of the blebs (Figure 2B, injection 1). The boundaries of the blebs appear as variably hypo-autofluorescent arcs that can be traced until the peripheral edge was out of reach to imaging. The SW-FAF outside of the bleb boundary showed a normally homogeneous gray background in the midperiphery crossed by the dark contour of the retinal vasculature, as well as the dark hypo-AF foveal center caused by absorption of the blue excitation light by the macular pigment.[36] Within the blebs there are striking changes with darker areas of non-homogeneous hypo-AF, some nearly circular, separated from the linear hypo-autofluorescent edge of the bleb by a band of better appearing, light gray, signal (for example, Figure 2B, injection 1). SW-FAF imaging after vector readministration in the eyes of the animal with the non-overlapping blebs replicated the same pattern observed after the initial administration (Figure 2B, injection 2). Partial overlap of the injected regions (BF54F) resulted in merging of the two blebs without a locally more severe loss of the autofluorescent signal within the overlapping section, whereas the animal with complete bleb overlap (11D086) showed denser hypo-AF within the bleb after readministration.

Spectral domain optical coherence tomography (SD-OCT) imaging was performed as *in vivo* microscopy of the retina (Figure 2C). Topographic maps of the thickness of the retina within the injected blebs performed after the initial injection are very similar to maps generated after readministration, suggesting no major changes in overall retinal thickness occurred for any of the three scenarios tested (non-overlapping, partially overlapping, and totally overlapping blebs) (Figure 2C). Particularly, topography maps straddling the boundary between uninjected and injected retina showed no abrupt transitions in thickness (which would indicate thinning within the bleb), but only a smooth transition to a thinner overall retina (cooler colors), which occurs normally with increasing distance from the fovea (uninjected regions, Figure 2C, injection 1). Closer inspection, however, reveals there were local changes in thickness within the blebs. Animal 10C015 shows an area of mild thickening in superior retina after the initial administration that is less obvious following readministration of the vector inferiorly (Figure 2C). This area corresponds to a whitish lesion on fundus photography (Figure 2A). Animal BF54F shows a band-like area of thickening superior to the nerve that also fades on follow up when the readministered bleb partially overlaps with this region. Animal 11D086, who had totally overlapping blebs following readministration, shows no differences in total retinal thickness topography before versus after readministration. The site of the retinotomy, which was used to reinject the same region, can be still seen as a local area of thinning highlighted in blue inferior to the nerve that turns slightly larger in maps after readministration (Figure 2C).

Histologic and Immunohistochemistry Correlates of *In Vivo* Micron-Scale Retinal Imaging

To gain a better insight of the structural changes, we selected single magnified SD-OCT cross-sections from the readministration (injection 2) and initial administration (injection 1) areas. These regions of interest (ROIs) included uninjected retina, boundary edge of the bleb, and areas that showed evident FAF abnormalities on *en face* imaging (Figure 2B). SD-OCT images were scaled and then aligned using vascular elements so that the images would be comparable in magnification, location, and orientation (Figure 3A). Nuclear layers (ONL, outer nuclear layer; INL, inner nuclear layer; GCL, ganglion cell layer) can be seen running as parallel hyporreflective bands bracketed by the highly reflective signals from the plexiform layers (OPL, outer plexiform layer; IPL, inner plexiform layer) and the retinal nerve fiber layer (RNFL), respectively (Figure 3A). The cross-section of superficial large blood vessels shows a hyperreflective image with posterior shadowing (Figure 3A, asterisk). Those were used to further align images from the first and second injections. Photoreceptor structures distal to the external limiting membrane (ELM) can be seen in cross-section, most noticeable among them at these pericentral/midperipheral locations were the signals originating from the inner segment ellipsoid band zone (EZ), the interdigitation between the tip of the photoreceptor outer segments (POSs) and the apical RPE (interdigitation zone [IZ], band), and RPE/Bruch's membrane (BrM). All cross-sections used for this analysis were located in near midperipheral supero-nasal and infero-nasal retina. At these locations, the cross-sectional profile is relatively flat, allowing for comparisons of relative thickness values of each of the retinal laminae

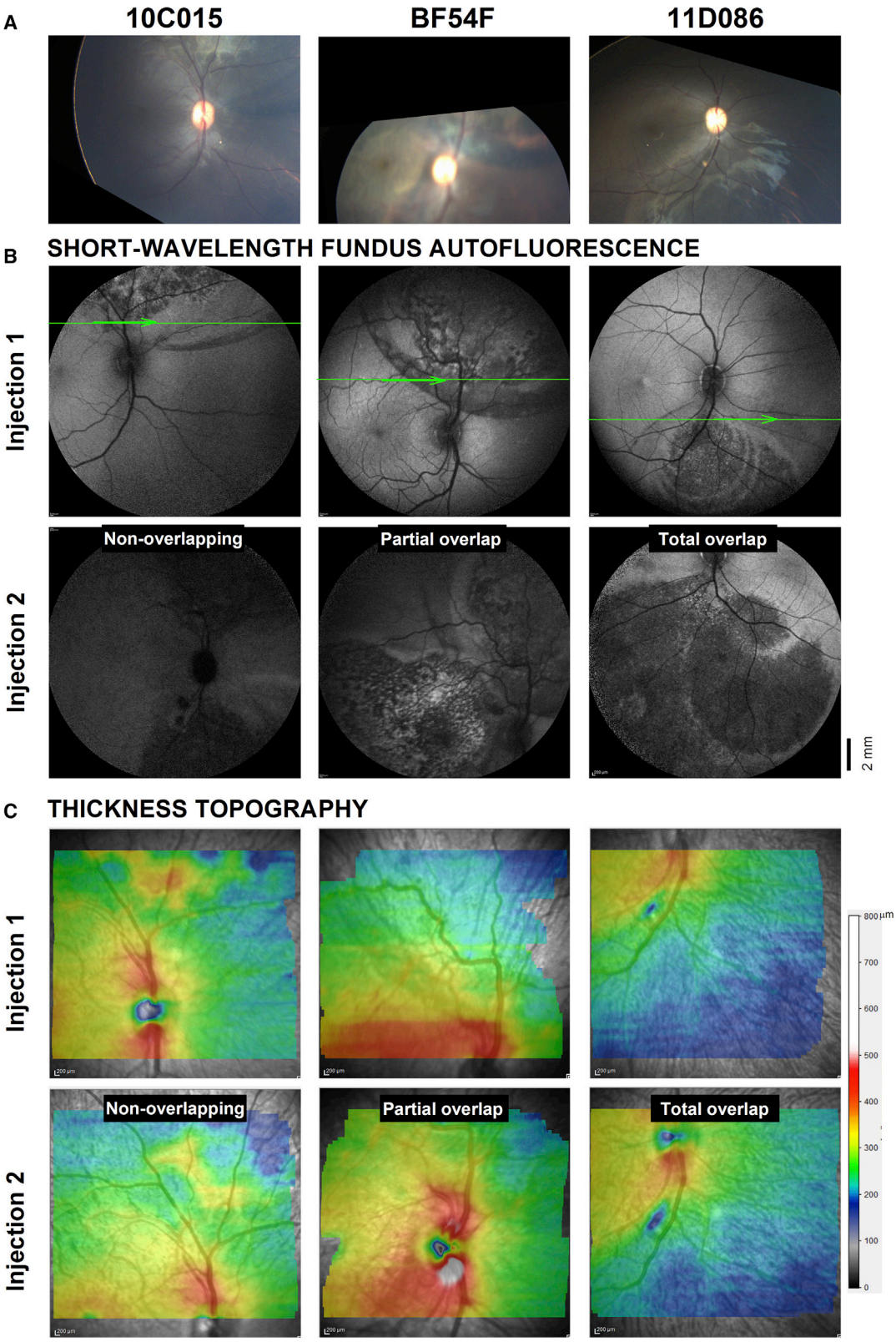

(legend on next page)

between locations inside the treated retina versus the surrounding untreated regions; the precise registration of the images from each eye between consecutive experiments was needed to assess for relative changes in thicknesses of each of the retinal sublaminae between the two injections.

Qualitatively, there were no obvious changes in any of the main nuclear, synaptic layers, or the RNFL layers in comparisons between uninjected and injected regions in any of the eyes for any of the two experiments or between the images taken after readministration compared to the same locations on initial administration (Figure 3A). However, closer inspection of the magnified SD-OCT cross-sections revealed various degrees of outer retinal sublaminae changes in the injected regions in most of the eyes. Changes included attenuation of the IZ and/or EZ band signals accompanied in some areas of disruption of the RPE signal by hyperreflectivities (for example, Figure 3A, animal BF54F). The changes occurred in blebs resulting from both the initial and the readministered injections and were apparently independent of the degree of overlapping of the blebs and of the degree of abnormalities in *en face* FAF imaging. For example, animal 11D086 with overlapping injections and the most severe abnormalities on SW- and near infrared-FAF (NIR-FAF) imaging showed the least changes on SD-OCT imaging at the locations sampled. Interestingly, re-emergence of the IZ band signal in 10C015 suggests some of the abnormalities may be transient, indicating recovery of the POS anatomy with time (Figure 2A). However, the disruption of the RPE band with apical hyperreflectivities may represent RPE depigmentation, hypertrophy, or migration and/or accumulation of subretinal inflammatory or degenerative debris.

At the time of necropsy, there were no abnormalities upon gross inspection in any abdominal or thoracic organs or in the brain. Histologic retinal sections obtained at study termination were chosen to closely match the locations represented in the SD-OCT to help understand the significance of the *in vivo* observations (Figure 2B). The histopathologic picture confirmed preservation of the nuclear layers and changes limited to the POS and the RPE consisting of examples of focal RPE hypertrophy that explain irregular hyperreflectivities superficial to the RPE on SD-OCT (Figures 3A and 3B, animal BF54F, white arrows). All NHPs showed dislodged or hypertrophic RPEs around the injection sites in at least one of their eyes, likely due to the mechanical nature of the injections. There was also mild focal loss of RPE cells or replacement of RPE cells by fibrinoid scar and a rare choroidal infiltrate (animal 11D86, right eye) that closely resembled the SD-OCT findings of loss of irregular hyperreflectivities superficial to the RPE (Figures 2A and 2B, animal BF54F, white arrows). There were examples of loss of RPE cells with replacement of RPE cells by fibrinoid scar and a rare choroidal infiltrate (Figure S1, animal 11D86, right eye). On histology, animal 11D086, which had almost completely overlapping injections, displayed shorter, yet reattached, POSs in some areas, but these didn't look disarrayed. Partially overlapping injection sites in BF54F showed areas lacking POSs in both eyes. Animal 10C015 also had areas lacking POSs in each of the non-overlapping blebs, but had longer, "cystic" POSs at the first injection site in the right eye.

Histopathology was graded from mild to severe according the number and distribution of inflammatory cells. Findings in NHPs BF54F and 11D086 were both categorized as generally mild and presented with occasional localized pockets of inflammatory cells in the choroid, but not in the subretinal space, suggesting these infiltrates did not have an impact on the retinas. NHP 10C015 exhibited focal inflammatory infiltrates in the subretinal space and therefore was classified as severe. No inflammation in the vitreous or the AC was observed in any of the animals. Quantitative SD-OCT parameters were used to assess for changes in thickness of the total retina, inner retina, and photoreceptor ONL, as well as for the EZ-to-BM distance, a surrogate measure for POS length (Figure 3C). The retinal cross-sections were segmented (see Materials and Methods; Figure 1) and thickness differences for each of the retinal laminae calculated either as a fraction of the thickness value in uninjected retina or as a fraction of the thickness value at the same location after the first injection. The aim was to facilitate comparisons between animals by avoiding expected regional differences in absolute thicknesses. Values were considered significantly different if they exceeded the inter-visit variability of the estimates (3SD = total, 6%; inner retina, 15%; ONL, 7%; EZ-BM, 18%) in uninjected NHP eyes.[37] There were no significant differences in thickness for total, inner, or ONL for any of the injected retinas compared to the neighboring uninjected retina or between the readministered regions compared to the initial administration, confirming qualitative observations (Figure 3C). Differences in total retinal thickness expressed as the fraction of the value measured after the initial injection showed mild thinning, nearly identical in injected (mean difference ± 2SD = −3% ± 6%) and uninjected (−2% ± 6%) regions (i.e., inside versus outside injection blebs) (paired t test, $p = 0.74$). Similarly, the EZ-BM distance showed non-significant thinning in both injected (−3% ± 13%) and uninjected (−6% ± 8%) ($p = 0.63$) retinas with the variability for the estimates of the injected retina (Figure 3C, red bar) driven by POS changes of animal BF54F. Comparisons between locations inside versus outside the injected blebs at the 1st injection or 2nd injection time points (Figure 3C, gray and black bars) were more variable reflecting expected normal topographic differences in thickness rather than real differences.

Figure 2. *En face* Retinal Imaging and Cross-Sectional Retinal Microscopy Obtained in Life for the Right Eye of Each of the Three Animals that Received Bilateral Readministration of AAV2-*hRPE65v2*

(A) Wide-angle color fundus photography of ocular fundus partially covering the injected regions. (B) Wide-angle (55 deg) SW-FAF of the same regions obtained after the first and second injections of the vector. Scale bar is at the bottom right. Superimposed thin green line is one of 62 horizontal raster SD-OCT scans use to generate maps of the overall retinal thickness topography in (C). The 9 mm × 7 mm maps straddle the boundary between injected and uninjected retina. Imaging was performed 1.5 months after each injection. Thickness values are plotted to a color scale (bottom right). Only right eyes shown for clarity; left eyes are virtually identical copies of the right eye.

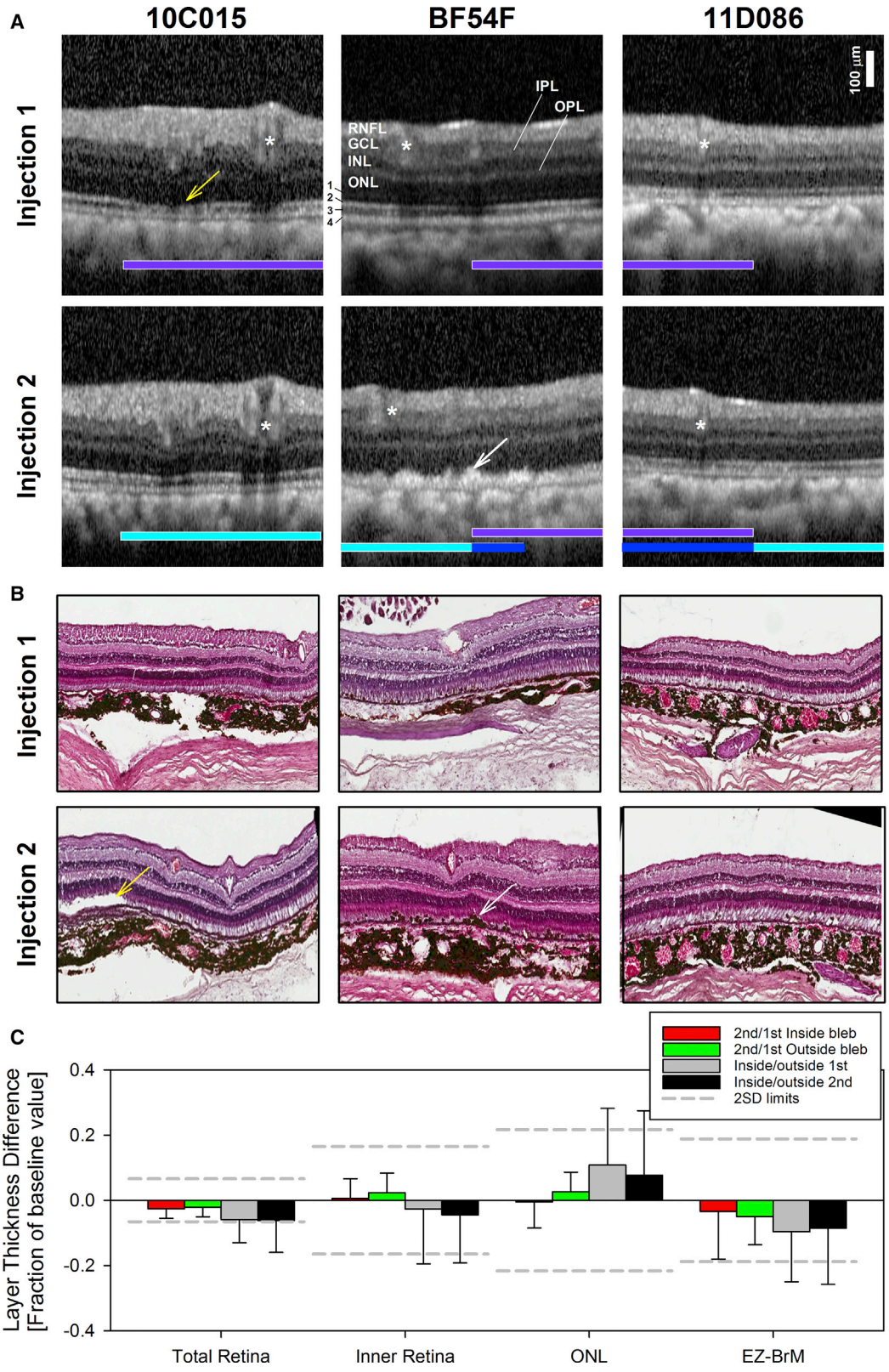

(legend on next page)

Outer Retina and RPE Changes after Subretinal Administration of AAV2-*hRPE65v2* in NHP but Not in Humans

Although there were no obvious differences in the structure of the inner retina and photoreceptor nuclear layer (i.e., ONL) after the first or readministered injections, there were changes in the POS and RPE that may not be readily visible on histology. Multimodal, *en face* retinal imaging with NIR-reflectance (NIR-REF), NIR-FAF, and SW-FAF, combined with co-localized cross-sectional *in vivo* histology with SD-OCT after the first injections were used to try to understand the origin of some of the abnormalities by imaging large retinal regions, which would not be easily sampled with histology (Figure 4). The contour of the injected bleb was not visible on NIR-REF on animal10C015, whereas they could be clearly seen in animals BF54F and 11D086 as round lighter areas of hypo-REF delimited from the uninjected retina outside of the bleb by a dark band. On NIR- and SW-FAF there was mottled hypo-AF near the center of the blebs, indicative of loss of melanin within RPE cells or loss of RPE cells and/or photoreceptors. Whereas the areas of abnormal FAF co-localized within the blebs using both excitation lights (NIR and SW), the area of NIR hypo-AF tended to be granular, more central, and not reaching the edge of the bleb, whereas on SW-FAF an abnormal hypo-AF signal may be tracked to the edge of the bleb (for example, Figure 4, animal BF54F). The center of these lesions on SW-FAF alternates normal (or hyper-FAF) with localized hypo-FAF, conferring the lesions a mottled appearance. Smaller circular contours or rings that are eccentric in relationship to the center of the bleb can be seen in one of the animals (Figure 4, animal 11D086). Magnified SD-OCT cross-sections across the transitional margin of AF changes revealed that the loss of the SW-FAF near the edge co-localized with the initial loss or attenuation of the IZ signal, whereas the loss of both NIR-FAF and SW-FAF signals correspond to the loss of the IZ signal and disruption of the RPE band (for example, Figure 4, BF54F). There were intraretinal hyperreflective tracks on SD-OCT above the RPE hyperreflectivities in BF54F (Figure 4, BF54F, *circled*). Of note, some of the hyper-FAF signals on SW-FAF co-localized with the presence of material above the RPE (Figure 4, animal 10C015, asterisk), whereas animal 11D086 shows minimal to no changes SD-OCT changes despite obvious hypo-AF on NIR- and SW-FAF. Immunohistochemical analysis using anti-RPE65 revealed a delineation between injected areas showing overexpression of RPE65 and untreated areas expressing endogenous RPE65 in all NHPs, although RPE65 protein was reduced in areas where there was RPE damage (Figure S3).

We delivered a subretinal injection of clinical grade voretigene neparvovec-rxyz to a patient with LCA caused by bi-allelic mutations (c.271C > T and c.725+2T > A) in *RPE65* and asked whether the FAF and SD-OCT abnormalities detected in NHP would be observed post-treatment in the patient. Of note, the procedure in patients, unlike in NHPs, is performed after a core vitrectomy, to prevent long-term complications, such as tractional retinal detachments.[12] The injection bleb in this patient covered the entire area of photoreceptor preservation on SD-OCT retinal thickness topography maps (Figure 5A). Given that SW-FAF signal is weak or absent in this condition NIR-FAF was favored for FAF imaging (Figure 5).[38–40] Before treatment there was a residual central oval island of relatively preserved NIR-FAF signal that corresponded with the detectable RPE and ONL signals on SD-OCT (Figure 5B). Repeat retinal imaging a month after the subretinal injections show nearly identical images on NIR-FAF, as well as on SD-OCT compared to baseline.

Defining the Immune Response on Same-Eye Readministration of AAV2-hRPE65v2 in NHPs

Baseline serum NAb titers to AAV2 ranged from negligible to high (Figure 6A), likely due to prior wild-type AAV2 exposure, which closely resembles the variation in AAV2 antibody titers observed in human sera.[24,26,27] As expected, none of the NHPs had a detectable antibody titer to the RPE65 protein at baseline as measured by ELISA. There were no changes in antibodies to RPE65 protein after the injections (data not shown). After the first bilateral subretinal injections, serum AAV2 NAb titers rose significantly in two of the three NHPs. One of them, BF54F, had a negligible titer at baseline. In the other, 10C015, titers rose from <1:100 to peak close to < 1:1,000, but dropped back down to baseline levels after the second injection. There were no observable changes in the remaining NHP (Figure 6A). Baseline NAb concentrations to AAV2 in the ACs averaged between the left and right eyes, were <1:10 in all three NHPs. Upon termination of the study, the AAV2 AC NAb titers had risen to <1:100 in BF54F and 1:1,000 in 11D086. There was no observable change in AAV2 antibody titers in the AC of BF54F (Figure 6B).

To assess T cell responses to the AAV2 capsid and RPE65 protein, we measured interferon-γ (IFN-γ) cytokine secretion using an enzyme-linked immunosorbent spot (ELISpot) assay on peripheral blood monocyte cells (PBMCs) collected at baseline prior to each subretinal injection and at 2-week intervals following the second injection

Figure 3. *In vivo* PII Micron-Scale Retinal Imaging and *Ex vivo* Histopathology

(A) Magnified, 2.3-mm-long, SD-OCT segments (horizontal thick arrows in Figure 2B) from a location ~1.5 mm from the optic nerve edge extracted from raster scans used to map a 9 × 7 mm area of retina at ~100 mm intervals in (C). Images were obtained 1.5 months after the first injection and second injections of the vector. Selected cross-sections sample the retina from uninjected to within the injected subretinal bleb that resulted from the first (overlaid horizontal violet bars) and second (turquoise bars) injections. Overlapping injected retinas shown as blue bars. Asterisks point to vascular landmarks used to ensure co-registration with *en face* SW-FAF images in (B), as well as to ensure the same region is evaluated on SD-OCT after the first and second injection. Neuronal nuclear (outer nuclear layer, ONL; inner nuclear layer, INL; ganglion cell layer, GCL) and axonal (retinal nerve fiber layer, RNFL) layers are labeled. Outer retinal sublaminae are numbered (1, ELM; 2, inner segment ellipsoid region band (EZ); 3, interdigitation zone (IZ) between the tip of the POS and the apical RPE; 4, RPE/BrM. (B) Representative H&E sections. White arrows point to hyperreflectivities superficial to the RPE on SD-OCT and hypertrophy and migration of RPE cells on histology. Yellow arrows point to attenuation of the IZ signal on SD-OCT and abnormal outer segments on histology. Only right eyes shown for clarity; left eyes are virtually identical copies of the right eye. (C) Comparison of quantitative structural SD-OCT parameters expressed as a fraction of the second/first injection time point values for injected ("blebs") (red bars) and uninjected (green bars) retina, as well as ratios of values measured inside/outside the blebs after the first (gray bars) and the second (black bars) injections. Error bars represent 2SD.Dashed lines delimits +-2SD of the intervisit variability of the parameter defined in uninjected retinas.

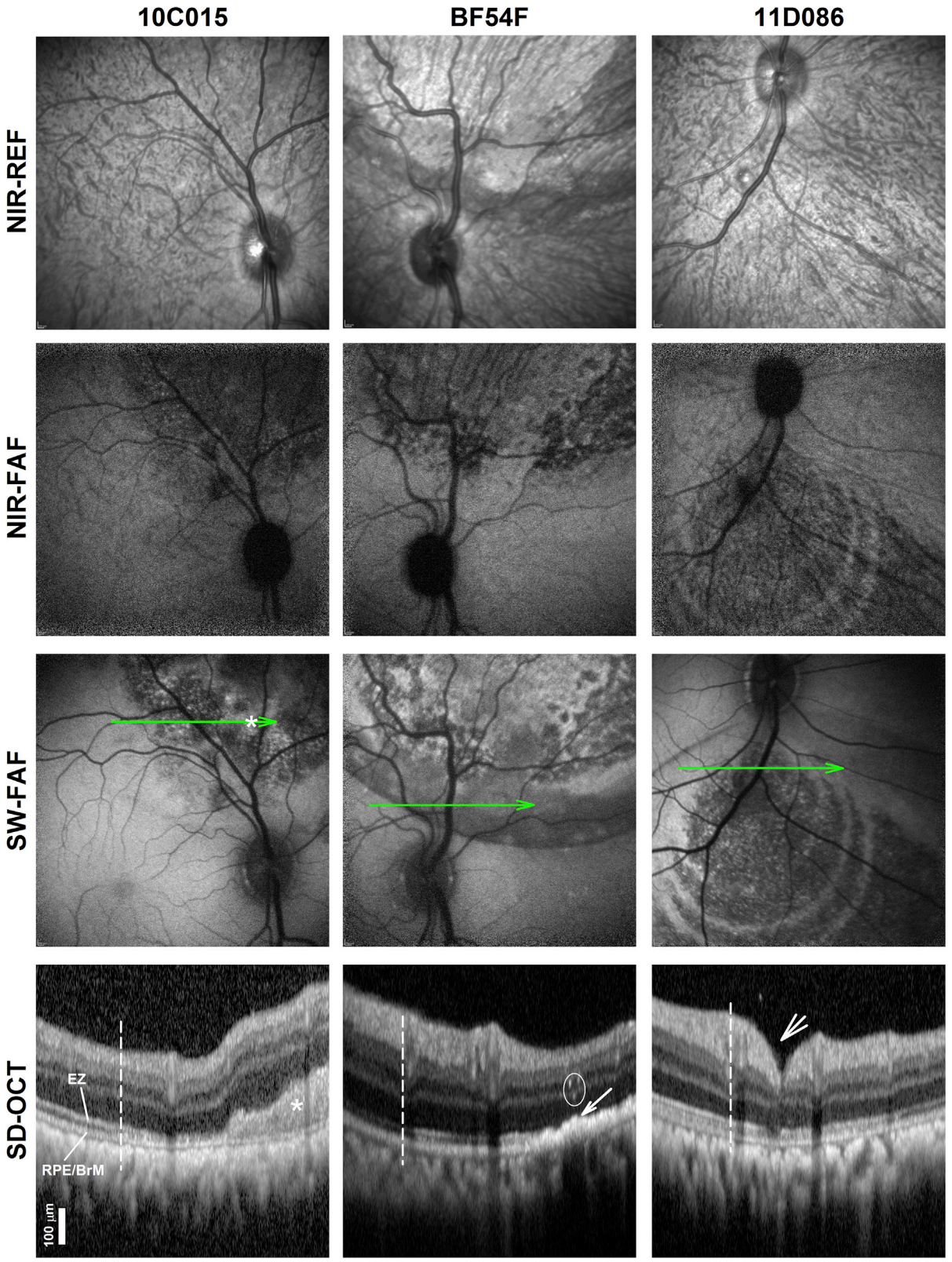

(legend on next page)

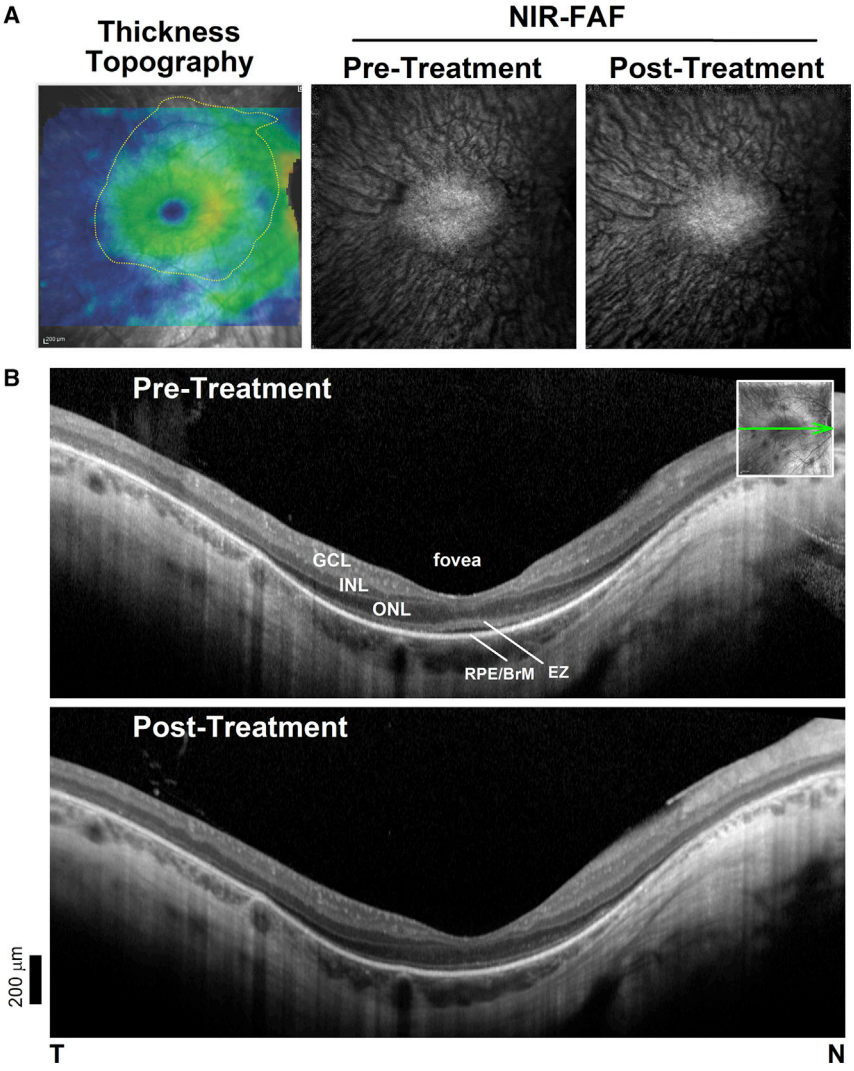

Figure 5. Imaging Studies after Administration of voretigene neparvovec-rzyl to a Patient with *RPE65*-LCA

Multimodal retinal imaging was performed as in the NHP experiments pre- and post-treatment. (A) SD-OCT total thickness tomography (left) and NIR-FAF pre- versus 1 month after treatment. Yellow contour denotes area with clearly detectable ONL (>10% or mean normal thickness) covered by the subretinal injection or bleb. (B) SD-OCT, 6-mm-long cross-sections through the fovea before and after treatment. Nuclear and outer sublaminae are shown as in Figure 3. Inset: NIR-REF image with an overlaying arrow to show the position and orientation of the scans. T, temporal; N, nasal retina. Scale bar bottom left.

(Figure 1). Cells were stimulated with AAV2 empty capsid particles and RPE65 peptide pools. Animal BF54F did not have a T cell response at baseline but developed a T cell response to the AAV2 capsid 4 weeks after the second administration of AAV2-*hRPE65v2* (Figure 7). This response decreased by the 6 week post-readministration time point. There was no significant T cell response to any of the RPE65 peptide pools.

DISCUSSION

The extraordinarily successful treatment of cases of childhood blindness (*RPE65*-associated IRD) by gene augmentation with AAV2-*hRPE65* has reenergized the entire gene therapy field with the approval by the FDA of this treatment (voretigene neparvovec-rzyl, Luxturna, Spark Therapeutics, Philadelphia, PA, USA) for use in the clinic in December of 2017. A phase III trial that supported this decision demonstrated robust and early improvements in retinal function in the majority of subjects (93%) after a single, localized, subretinal injection of the therapeutic agent in each eye. Sensitivity to light post-treatment increased on average by about 100-fold, supporting enlarged visual fields that permitted better obstacle avoidance and overall improved quality of life.[11] The trial further confirmed the treatment's safety. Complications included temporarily elevated intraocular pressure, cataracts, retinal tear (10% of participants), macular hole (one eye of one participant), and decreased foveal function (albeit improved extrafoveal light sensitivity, one participant), all of which have been attributed to the intraocular surgical procedure needed for the delivery of the recombinant virus to the subretinal space, including a vitrectomy, the creation of a localized retinal detachment, and then a fluid-air exchange within the vitreous cavity. The phase III trial included bilateral administration since safe and successful treatment of the contralateral eyes of previously treated (uniocularly) *RPE65* patients had been demonstrated.[22–24] Readministration of a gene therapy vector to a previously treated eye or region within a tissue such as the retina, however, is an unavoidable subject that has not been explored experimentally in the retina and which has only been limitedly addressed elsewhere.[41,42] Scenarios where same eye readministration may be indicated include

Figure 4. Outer Retinal Changes Evaluated by *En face* and Cross-Sectional SD-OCT Retinal Imaging

En face NIR REF and FAF imaging with NIR and SW excitation lights. Representative 2.3 mm magnified SD-OCT cross-sections through the boundary (vertical dashed lines) of the injected blebs. Green lines on *en face* imaging represent the location and orientation of the SD-OCT scans. Nuclear layers and outer retinal sublaminae labeled in Figure 3. Asterisks denote subretinal hyperreflective image that may correspond to deposits and/or fibrosis observed on histology and hyper-FAF. Arrow points to hyperreflectivities apical to a disrupted RPE/BrM band that should correspond to RPE abnormalities described on histology. Circle, intraretinal linear reflectivities reflecting intraretinal pigment migration and/or reactive gliosis/Muller cell hypertrophy. Short arrow, retinotomy.

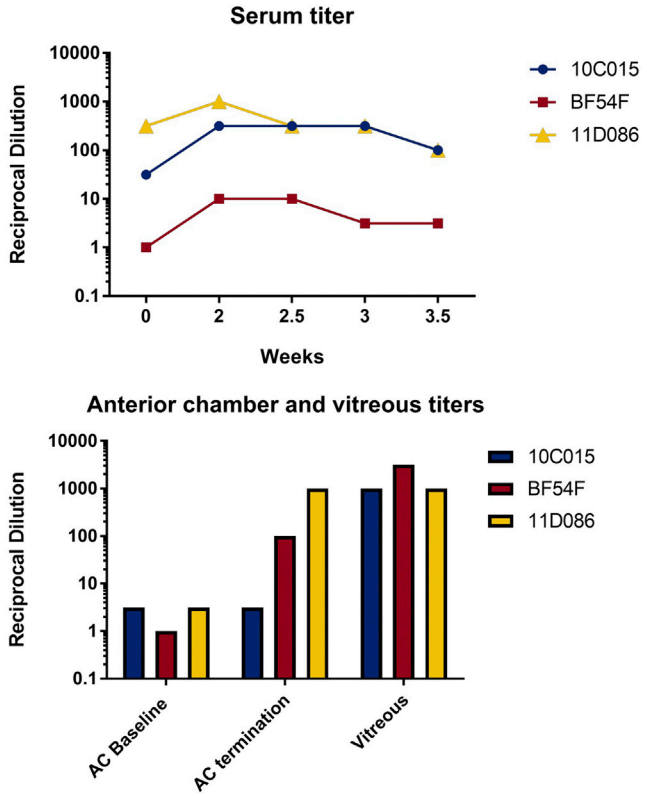

Figure 6. Serum Anti-AAV2 Nab Titers Rose Significantly in Two of the Three NHPs after Bilateral Subretinal Injection of AAV2-hRPE65v2

(A and B) NAbs to AAV2 capsid in (A) serum and (B) AC fluid at baseline and at various time points following the first subretinal injection. Serum NAb (A) and average NAb titers calculated for both eyes in AC fluid and vitreous samples (B) from baseline prior injection #1 (week 0) through the end of the study. All NHPs had high AAV2 NAb titers present in the vitreous of both eyes upon termination (vitreous could not be collected at baseline due to the invasiveness of the procedure).

the treatment of untreated regions to further expand vision, the treatment of regions that may be purposely spared during a staged treatment protocol where the frailty of the degenerated retina is tested in visually non-sensitive areas before extending the treatment to include critical areas for vision, such as the central retina, and as a treatment booster should a decline in efficacy be detected over time.

In the present study we used *in vivo* multimodal retinal imaging, measures of cellular and humoral immunity, and histopathology to explore the consequences of ipsilateral readministration of rAAV2-*hRPE65v2* in NHPs. The uncomplicated treatment in patients leaves minimal visible evidence just a few days or weeks after the injections. In contrast, the administration of rAAV2-*hRPE65v2* to NHPs produces pigmentary changes within the blebs visible by fundus exam, which can be used to precisely locate a second subretinal injection in relationship to a previous one. In one animal (two eyes), a readministration of the treatment was at a site distant from the first injection to exclude mechanical (surgery-related) effects on the initially injected retina; in the other two animals, the treatment was delivered so that there was a partial or total overlap between the first and second injections.[13,43] The experiments demonstrated that ipsilateral readministration to the NHP retina was safe from an immunologic standpoint, even when readministration location coincided nearly exactly with the initially treated retinal area. Repeat injections were well tolerated even though the initial injection had resulted in an increase in systemic and local neutralizing antibodies to the AAV2 capsid in two of the animals. There were no clinical signs of inflammation and the ocular media remained clear even though the animals had not been treated with systemic steroids.

In vivo multimodal retinal imaging allows quantitation of the microscopic structure over large expanses of retina, overcoming potential under-sampling and/or simplifying the sampling process that would be required with histology.[44] Structures in the outer retina, such as the POS, as well as potential changes in the content of certain fluorophores within the RPE, such as lipofuscin and melanin, can be readily assessed *in vivo*, details that can only be viewed with histology after laborious tissue processing. SD-OCT after the initial administration or readministration of rAAV2-*hRPE65v2* revealed no obvious signs of intraocular inflammation such as hyperreflective images within the vitreous or the retina that would suggest migration of inflammatory cells or the presence of overt infiltrates. There were, however, examples of subretinal images that may correspond to accumulation of subretinal material, including inflammatory cells, migrated RPE cells and/or shed unphagocytized outer segments. The most consistent and dramatic change on imaging was the presence of round areas of hypo-AF (on SW- and NIR-FAF imaging) within the blebs that corresponded with loss of the IZ signal suggesting POS abnormalities or loss and demelanization of the RPE.[45] Readministration of the vector in the overlapping blebs led to overlapping additional depigmentation but did not lead to worsening of the existing changes. The photoreceptor nuclear layer and the inner retina had a normal appearance, confirming that the abnormalities were compartmentalized to the subretinal space exposed to the treatment. Regions of RPE loss were negative for RPE65 protein by immunohistochemistry suggestive of RPE loss or damage, although neighboring regions with intact RPE showed robust presence of RPE65. Abnormalities of this magnitude have not been reported in humans after subretinal gene therapy for *RPE65* deficiency, although versions of this appearance are known to occur after persistent submacular retinal detachments.[14,46] Similarly, a patient treated with voretigene neparvovec-rzyl and imaged in this study did not show demelanization or loss of the POS. Thus, the abnormalities after subretinal injection of this particular reagent/dose appear to be NHP-specific.

Histopathology of the ipsilateral readministered injections at the termination of the study showed a pattern indistinguishable from earlier descriptions following a one-time subretinal administration of gene therapy products in NHPs.[18,31,47–49] Histopathologic changes included RPE hyperplasia, focal RPE loss, and proliferation. Of note, the immunologic profile was not predictive of the histological abnormalities and did not relate to the overlap between the initial and re-administered treatment. For example, the most severe inflammation

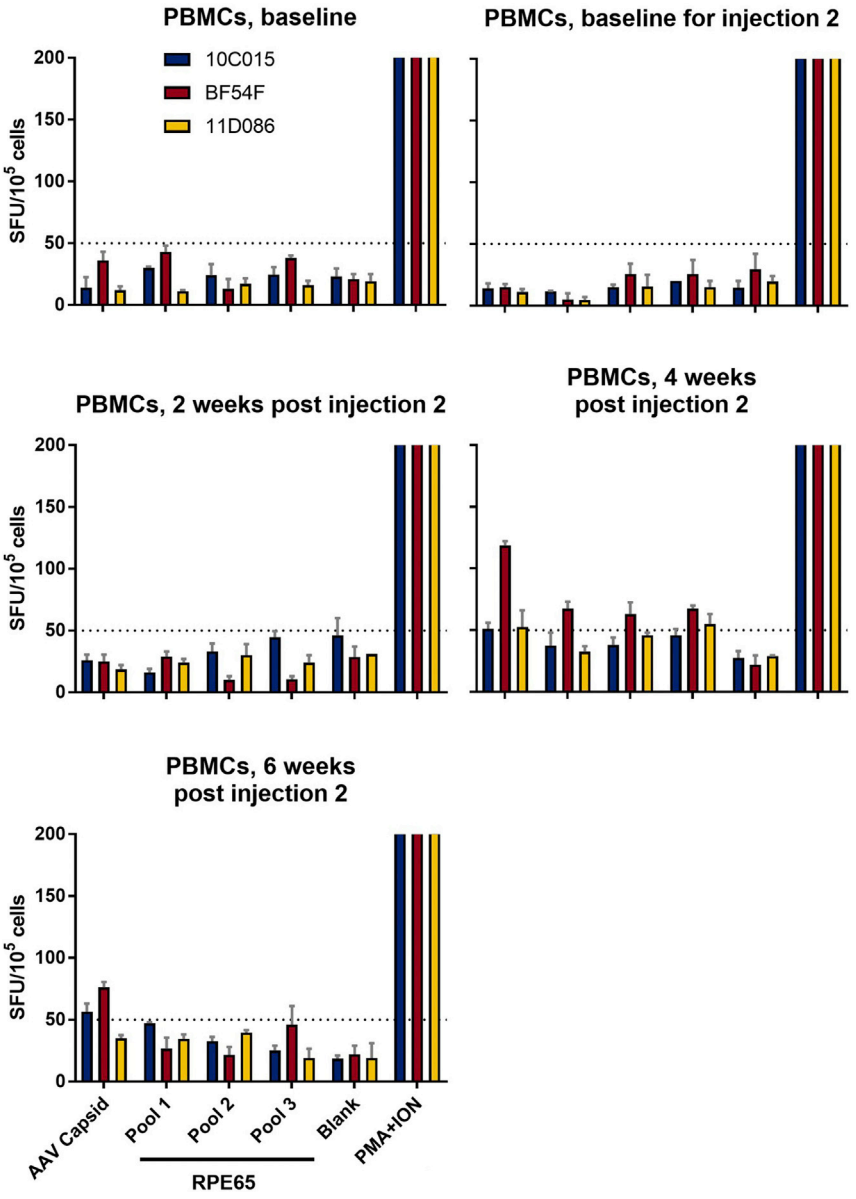

Figure 7. T Cell Responses Directed against AAV2 Capsid or the RPE65 Protein as a Function of Time after Ipsilateral Subretinal Readministration of AAV2-hRPE65v2

IFN-γ secretion by PBMCs after stimulation with the AAV2 capsid or RPE65 protein at baseline and post-injection time points showed variable increases at the 4 week time point as measured by IFN-γ ELISpot assay with PMA+ION, positive control. The different test antigens for each of the panels are indicated in (E). The pre-injection samples (baseline and baseline for the first injection) are shown in (A) and (B), respectively. The results at 2, 4, and 6 weeks post injection 2 are shown in (C), (D), and (E), respectively. One animal showed a cell-mediated response to the AAV capsid at the 4 week time point (D) and that response then subsided (E). There were also cell-mediated responses to the RPE65 protein at 4 weeks (D) and those resolved thereafter (E). Response to an antigen was considered positive when the number of SFUs per 200,000 PBMCs was higher than 50 SFUs (dotted line) per 200,000 PBMCs and three or more times the SFU per 200,000 PBMCs measured for the medium control. Error bars indicate SEM, calculated as the SD of the readings divided by the square root of the number of readings.

was observed in the retinas of the animal in which the blebs did not overlap (10C015). Specifically, there were dislodged RPE cells, which were hypertrophic and showed signs of RPE proliferation. In some areas, the border between the RPE and the underlying BM was blurred, which corresponded with retinal imaging findings suggestive of RPE loss and proliferation discussed before. At baseline, this animal did not show evidence of cell-mediated immune response to AAV2, although it did have baseline humoral anti-AAV2 NAbs (reciprocal dilution of >1:10). The inflammation was localized to small focal regions in the choroid underlying the original bleb sites and did not spill into the overlying retina, suggesting a compartmentalized response. There was no evidence of cellular infiltrate that might have been directed at the recombinant AAV or the RPE65 transgene product, except for within isolated pockets in the choroid despite prior exposure to AAV2 based on baseline serum titers. On the other hand, the animal with total overlap between the second and first injection showed the least structural change, whereas the animal with the highest baseline NAb titer directed against AAV2 (11D086) showed the mildest histologic changes after readministration (mild RPE pigment migration and focal RPE disorganization, one mild focal site of choroidal inflammation). Only one animal that had baseline NAb titers to AAV2 (BF54F) developed cell-mediated immune responses to AAV2 4 weeks after the second administration—around the time when an immune response would be expected to be close to maximal—and again the structural change after readministration was indistinguishable from the other two animals.

Dose-dependent outer retinal changes with demelanization of the RPE have been reported after the administration of different vector constructs in NHPs, as well as after injection of control balance salt solutions.[37,43,47,48] These vector-independent abnormalities may be the consequence of low grade, immune-mediated responses within the subretinal space triggered by exposure of foreign proteins that may not be detected by the immune assays used in this work or by routine histopathology. The pigmentary changes post-administration in NHPs noted on fundus examination as early as 72 h post-treatment raise the alternative possibility of acute damage to a particularly

susceptible NHP POS and/or RPE to the separation between the layers caused by the subretinal injection.[43,47] The circular, ring-like autofluorescent patterns documented in these NHP experiments may represent steps of bleb formation or reabsorption that may not occur in humans (for example, Figure 4, animal 11D086; Reichel et al.[48]). Such steps may be expected if greater hydraulic forces are required in NHPs compared to humans to overcome the adhesion between the retina and the RPE, which in turn may result in uneven rates of delivery of the subretinal injections.[47,50–53] In fact, efforts are underway to de-risk the subretinal injections in patients with the use of mechanical devices that deliver precise volumes at prescribed hydrostatic pressures, as well as with the use of intraoperative SD-OCT systems that allow real time view of the microscopic retinal structure during the surgical interventions.[52,54] Experiments in NHPs following similar precautions are needed to narrow down the possible causes.[43] The findings are relevant for the interpretation of experiments where foreign proteins are delivered by gene therapy in NHP retinas in preclinical assays of safety, as well as for gene therapy treatments that are being conducted in patients. Although the exact mechanism(s) that lead to these abnormalities are yet to be fully elucidated, limited POS and RPE changes may be expected in similar experiments and may not necessarily indicate an unsafe treatment for patients.[37,43,47–49,55,56] Monitoring the health of the injected retina in patients is thus warranted particularly when the target outcome of the retinal gene therapy procedure lies distant to the treated regions, such as in applications where gene therapy is used to produce secretable proteins, because damage or loss of transfected retinal tissue may lead to the loss of the gene product and treatment efficacy.[37,57] On the other hand, comparatively mild but potentially visually significant changes in the outer retina reported after subretinal gene therapies underscore the need for a better understanding of the pathophysiology of the outer retinal abnormalities after subretinal delivery of gene therapies in NHPs and in patients.

As noted above, structural changes following the subretinal injection in NHPs treated with AAV2-*hRPE65v2* appear to differ in important ways from the observations in patients. Could the differences be explained by differences in the surgical procedures and peri-operative medications used in human subretinal surgery versus the NHP studies reported in this work? Humans are expected to survive this intervention for decades, as opposed to just months in the NHP experiments. A vitrectomy is performed in patients as a step prior to the subretinal injections to reduce the risk of post-surgical vitreoretinal adhesions and tractions. A similar procedure in the smaller NHP eye would increase the risks of procedural complications confounding the interpretation of potential vector-related toxicity. Similarly, the surgical complexity of smaller eyes has limited the approval of voretigene neparvovec-rzyl for use in human infants. The less traumatic procedure in NHPs predicts less rather than more structural changes and would not explain the localized, both in extent (within the bleb), as well as in depth (at the POS and RPE), structural abnormalities observed post-injection. Human subretinal injections delivering AAV2-*hRPE65v2* in phase I–III trials or after FDA approval of voretigene neparvovec-rzyl also include peri-operative treatment with prednisone, whereas no systemic steroids were used in the present NHP studies. In this work they were purposely omitted to avoid interference with the development of an immune response and inflammation after ipsilateral readministration of the vector. Thus, the results from this preclinical study in NHPs likely reflect what would be the "worst-case" scenario of ipsilateral readministration in humans. Studies controlling for these variables are needed to understand the differences between the human and NHP outcomes.

In summary, the results support the overall safety of the ipsilateral readministration of AAV2-*hRPE65v2*. Localized structural abnormalities confined to the outer retina and RPE after readministration of the treatment in NHPs do not differ from those observed after single or contralateral administration of this therapy. The structural changes observed after administration of AAV2-*hRPE65v2* in NHPs contrast from the unchanged appearance of the human retina exposed to the same vectors, suggesting there may be local immunologic responses in NHPs retinas after the subretinal injections that escape detection with current assays, and/or differences between human and NHP outer retinas that influence the response to these treatments. Documentation of the immunologic profile, of the dynamics of subretinal fluid entry and reabsorption from the subretinal following single injections in NHPs, testing control vehicles without viral capsids, and the evaluation of outcomes with and without immunosuppression, as well as the use of more locally sensitive immunologic assays, are needed to narrow down the alternatives.

MATERIALS AND METHODS

Animals, Study Design, and Ocular Surgery

The studies were in compliance with local and federal guidelines and were carried out under an Institutional Review Board approved protocol (The Children's Hospital of Philadelphia, IACUC protocol 1061, and the University of Pennsylvania IRB protocol 815348) and were in accordance with the ARVO Statement for the Use of Animals in Ophthalmic and Vision Research (Association for Research in Vision and Ophthalmology, Rockville, MD). NHPs were selected for study due to similarities to humans in ocular anatomy, vision, and immune response.

The study was conceived as a prospective observational study. Included were three 7- to 9-year-old NHPs—two cynomolgus and one rhesus macaque primate. After a baseline evaluation (see below), each animal received subretinal injections of the study agent in each eye followed 2 months later by readministration of the same agent to each eye (Figure 1). The subretinal injection procedure was carried out using sterile instrumentation, surgical fields, and injectable and topical medications. The NHP eye is ~70% the diameter of the mature human eye, approximately the size of that of an infant.[58] The smaller eye size increases the risk of complications due to vitrectomy and fluid-air exchange used in the human surgery, and in fact justifies the exclusion of infants from the FDA-approved use of Luxturna.[12] In this study, we felt that a better understanding of the toxicity could be gained by performing the less invasive, lower risk

procedure. The subretinal injections were thus administered without a previous vitrectomy but the procedure was otherwise identical to that used in patients.[12,24] The injections were performed under direct visualization through an operating microscope after an AC paracentesis (ACP) following procedures detailed elsewhere.[24] In brief, a needle was inserted through a trocar, introduced by sclerotomy, at the 2 or 10 o'clock position, which was then advanced through the vitreous to penetrate the retina in the posterior pole. Under microscopic control, 100–200 μL of the agent (resulting in doses of 1.0–2.0 E^{11} vector genomes [vg]) was manually injected into the subretinal space, thereby raising a dome-shaped retinal detachment (bleb). This dose was similar (within one half a log unit) to the dose used in the phase III RPE65 clinical trials carried out at The Children's Hospital of Philadelphia and University of Iowa and as recommended for treatment with Luxturna, 1.5 E^{11} vg. The solution was not drained, but was resorbed within a few h by the retina. The sclerotomy site was sutured with absorbable suture. After each procedure, a subconjunctival injection of 15 mg of Kenalog solution (40 mg/mL) was delivered and the ocular surface was dressed with PredG (prednisolone acetate-gentamicin, 0.3%/0.6%; Allergan) ointment. Other than that, no immunosuppression was administered. Ophthalmoscopic examinations were carried out prior to and immediately following subretinal injection, post-operative day 3 for each injection, and prior to euthanasia (Figure 1). Venous blood was collected at baseline before the subretinal injections, at 2 week intervals following the readministration and at termination of the study. PBMCs and sera were isolated from the venous blood samples. The PBMCs were purified and stored in vapor phase liquid nitrogen, and sera were frozen at −80°C until testing. Aqueous humor samples to measure AAV-capsid-specific antibodies were obtained by ACPs at scheduled intervals (Figure 1). ACPs were performed in a sterile manner using a tuberculin syringe attached to a 30G hypodermic needle; a maximum of up to 100 μL of aqueous fluid was collected. At the termination of the study, animals were euthanized and samples collected for immune assays, immunohistochemistry, and histopathology (Figure 1).

Study Agent

AAV2-*hRPE65v2* contains *hRPE65* cDNA under control of a constitutive promoter (a hybrid chicken β-actin promoter with a cytomegalovirus enhancer) and a long stuffer sequence designed to prevent reverse packaging.[10] This is the same plasmid that was used to generate the reagent used in phase I, follow-on, and phase III clinical trials for RPE65 deficiency at The Children's Hospital of Philadelphia and the University of Iowa as well as the now commercially available vector (voretigene neparvovec-rzyl, Spark Therapeutics, PA, USA).[11,12,22,23,59] The rAAV used in this study was manufactured by the Research Vector Core at the Center for Advanced Retinal and Ocular Therapeutics (CAROT) at the University of Pennsylvania Perelman School of Medicine—not Spark Therapeutics—and so is termed AAV2-hRPE65v2 to avoid confusion with the GMP-generated reagent. The virus was manufactured after triple transfection of HEK293 cells and was isolated and purified by microfluidization, filtration, cation exchange chromatography (POROS 50HS; HE Healthcare, Piscataway, NJ, USA), density gradient ultracentrifugation, and diafiltration in PBS. This combination provides highly purified, transgene cassette-containing AAV particles and efficiently removes empty capsids and residual cesium chloride. The purified virus, along with 0.001% Pluronic F-68 (PF68; BASF, Ludwigshafen, Germany), was then passed through a 0.22-μm filter and stored frozen (–80°C) in sterile tubes until use. Quality control procedures included SDS-PAGE and silver staining (for vector purity), quantitative real-time PCR (to assess vg concentration), osmolality, pH, and endotoxin testing.

In vivo Retinal Imaging

Retinal imaging was performed in fully anesthetized animals. A heating pad maintained body temperature during the experiments. Vital signs were monitored periodically with a pulse oximeter and rectal thermometer. At the completion of procedures, animals were monitored closely through recovery. Pupils were dilated with topical tropicamide (1%) and phenylephrine (2%). Eyes were kept opened with an eye speculum inserted after topical anesthesia with proparacaine-HCL (1%). Corneal lubrication and clarity were ensured by frequent instillation of preservative-free artificial tears. Retinal imaging was performed 1.5 months after the first post-injection and 1 month after the readministration (Figure 1). *En face* retinal imaging was performed with NIR (790 nm) REF and FAF with NIR (820 nm) and SW (488 nm) excitation lights using a commercially available scanning laser ophthalmoscope camera integrated with a SD-OCT system (Spectralis, Heidelberg Engineering, Carlsbad, CA, USA). Overlapping *en face* imaging fields were collected with 30° and 55° lenses extending into the midperiphery to cover as much as possible the injected regions. Color fundus photography was performed with a wide-angle contact lens system (RetCam3 instrument, Natus Medical, Pleasanton, CA, USA). SD-OCT scanning was performed with 9 mm-long horizontal and vertical cross-sections through the fovea and overlapping 30° × 25° mm raster scans extending into the near midperiphery. Histological retinal laminae were quantified with the built-in automatic segmentation of the Spectralis system, supervised to ensure correct identification of the different laminar boundaries by visual inspection and with the use of longitudinal reflectivity profiles (LRPs) extracted with available analysis software (ImageJ; https://imagej.nih.gov/ij/; provided in the public domain by the NIH, Bethesda, MD, USA).[45] Total retinal thickness topography maps were generated, which in conjunction with *en face* imaging (NIR-REF and NIR-FAF) were used to visualize the treated regions as ROIs where a more focused analysis of the segmentation took place. Segmentation parameters examined within ROI included: 1, total retinal thickness, defined as the distance between the internal limiting membrane (ILM) and the basal side of the RPE signal at the level of the BM; 2, inner retinal thickness, defined as the distance between the ILM and the OPL; 3, ONL thickness, defined as the distance between the OPL and the ELM; 4, EZ band to the RPE/BM, defined as the distance between these two bands on SD-OCT.[37,44] Smaller regions within the ROI that co-registered as judged by co-registration of vascular landmarks before and after treatment were similarly scaled and rotated and comparisons were made between pre- and post-injection parameters.

Necropsy, Histopathology, and Immunohistochemistry

At the conclusion of the studies, animals were euthanized, AC fluid and vitreous samples were collected, and eyes were enucleated. The globes were fixed 24 h in 4% paraformaldehyde in PBS before OCT embedding and cryosectioning. The posterior pole was isolated. Retina and underlying RPE/choroid were cryoprotected in 30% sucrose in PBS and frozen. Cryosections were made at 12 μm and designated sections were stained with DAPI or processed for immunohistochemistry for RPE65.

Immunohistochemistry was carried out using a rabbit anti-mouse RPE65 (Novus Biologicals, Centennial, CO, USA) and a horseradish peroxidase-conjugated anti-mouse secondary antibody (Amersham, Little Chalfont, United Kingdom) prior to DAB staining with kit (Abcam, Cambridge, MA, USA) or stained with H&E. Slides were evaluated in a masked fashion by a board-certified ocular pathologist (V. Lee).

ELISpot Assays

IFN-γ assay on PBMCs were performed as previously described.[24] Response to an antigen was considered positive when the number of spot-forming units (SFUs) per 200,000 PBMCs was higher than 50 SFUs per 200,000 PBMCs and three or more times the SFU per 200,000 PBMCs measured for the medium negative control. Phorbol myristate acetate (PMA) was used at a final concentration of 5 ng/mL with ionomycin at 2 mM as a positive stimulant to ensure an equivalent number of functional T cells per well. For the experimental reagents, RPE65 peptide libraries were generated by Mimotopes (Minneapolis, MN, USA) and consisted of 105 overlapping 15-mers. Purified empty AAV2 capsids were used to test cell-mediated responses to the AAV capsid as previously described.[12] SEMs were calculated as the SD of the readings divided by the square root of the number of readings.

NAb Assay and ELISA Antibody to AAV2

NAb titer to AAV2 was determined as previously described with a β-galactosidase assay.[24] The positive control was maximal transduction of AAV2-LacZ without the addition of serum to the sample, while the negative control contained buffer only. Human sera samples previously assayed to be positive for antibodies to the AAV2 capsid were used as reagent controls.[24]

ELISA for Antibodies to RPE65

Antibody titer to RPE65 was determined with an ELISA by modification of previously described methods.[10,23,24] The positive control was the PETLET rabbit anti-mouse RPE65 antibody (gift of Dr. Michael Redmond). The titer was defined as the reciprocal of the highest sample dilution such that the mean optical density for the test antigen was at least three times that for the control antigen and at least three times the background level, determined from the buffer-only negative control. BSA was used as a negative antigen control.

Treatment in Human

A single individual with *RPE65*-LCA was treated clinically with AAV2-*hREP65v2* (voretigene neparvovec-rzyl, Luxturna, Spark Therapeutics, Philadelphia, PA, USA) and imaged with SD-OCT and FAF as previously described.[44] The treatment administration and imaging protocol used in the NHP experiments were delivered following the protocols used in patients using similar surgical technique and the same imaging instrumentation.[12,44,60] Informed consent was obtained both clinically and for the imaging portion of the study after explanation of the nature of the study. Procedures complied with the Declaration of Helsinki and were approved by the institutional review board of the University of Pennsylvania (IRB #815348).

SUPPLEMENTAL INFORMATION

Supplemental Information can be found online at https://doi.org/10.1016/j.omtm.2019.08.011.

AUTHOR CONTRIBUTIONS

L.W., J.B., and T.S.A. conceived the study, designed and generated reagents, performed experiments, analyzed data, and wrote the manuscript. T.S.A performed experiments and collected data. M.J.A. and L.W.S. assisted with data analyses. S.Z., A.M.M., and Z.Y. carried out technical procedures. V.L. evaluated the histopathology. J.S. reviewed the immunology. All authors edited and approved the finalized manuscripts.

CONFLICTS OF INTEREST

J.B. and A.M.M. are co-authors on a patent relevant to development of gene therapy for *RPE65* deficiency (US Patent #8,147,823) but waived any potential financial gain in 2002.

ACKNOWLEDGMENTS

We thank Vibha Anand Jawa for thoughtful comments and suggestions. We thank the Center for Advanced Retinal and Ocular Therapeutics Research Vector Core for production of the rAAV vector and Roberto Calcedo, Valder Arruda, and Leon Morales for assistance with immune assays. We are grateful to Drs. Travis Seymour, Dorian Culmer-Butler, Benoit Mermoud, and Mary Kate Goldy for their expert care of the animals. Funding is supported by the Center for Advanced Retinal and Ocular Therapeutics (CAROT), The Brenda and Matthew Shapiro Stewardship, the Robert and Susan Heidenberg Investigative Research Fund for Ocular Gene Therapy, The Pennsylvania Lions Sight Conservation and Research Foundation, The Paul and Evanina Bell Mackall Foundation Trust, and Research to Prevent Blindness.

REFERENCES

1. Verbakel, S.K., van Huet, R.A.C., Boon, C.J.F., den Hollander, A.I., Collin, R.W.J., Klaver, C.C.W., Hoyng, C.B., Roepman, R., and Klevering, B.J. (2018). Non-syndromic retinitis pigmentosa. Prog. Retin. Eye Res. *66*, 157–186.

2. Wright, A.F., Chakarova, C.F., Abd El-Aziz, M.M., and Bhattacharya, S.S. (2010). Photoreceptor degeneration: genetic and mechanistic dissection of a complex trait. Nat. Rev. Genet. *11*, 273–284.

3. Weleber, R.G., Francis, P.J., Trzupek, K.M., and Beattie, C. (2013). Leber Congenital Amaurosis (University of Washington).

4. Redmond, T.M., Poliakov, E., Yu, S., Tsai, J.Y., Lu, Z., and Gentleman, S. (2005). Mutation of key residues of RPE65 abolishes its enzymatic role as isomerohydrolase in the visual cycle. Proc. Natl. Acad. Sci. USA *102*, 13658–13663.

5. Redmond, T.M., and Hamel, C.P. (2000). Genetic analysis of RPE65: from human disease to mouse model. Methods Enzymol. *316*, 705–724.

6. Redmond, T.M., Yu, S., Lee, E., Bok, D., Hamasaki, D., Chen, N., Goletz, P., Ma, J.X., Crouch, R.K., and Pfeifer, K. (1998). Rpe65 is necessary for production of 11-cis-vitamin A in the retinal visual cycle. Nat. Genet. *20*, 344–351.

7. Marlhens, F., Bareil, C., Griffoin, J.M., Zrenner, E., Amalric, P., Eliaou, C., Liu, S.Y., Harris, E., Redmond, T.M., Arnaud, B., et al. (1997). Mutations in RPE65 cause Leber's congenital amaurosis. Nat. Genet. *17*, 139–141.

8. Gu, S.M., Thompson, D.A., Srikumari, C.R., Lorenz, B., Finckh, U., Nicoletti, A., Murthy, K.R., Rathmann, M., Kumaramanickavel, G., Denton, M.J., and Gal, A. (1997). Mutations in RPE65 cause autosomal recessive childhood-onset severe retinal dystrophy. Nat. Genet. *17*, 194–197.

9. Cideciyan, A.V. (2010). Leber congenital amaurosis due to RPE65 mutations and its treatment with gene therapy. Prog. Retin. Eye Res. *29*, 398–427.

10. Bennicelli, J., Wright, J.F., Komaromy, A., Jacobs, J.B., Hauck, B., Zelenaia, O., Mingozzi, F., Hui, D., Chung, D., Rex, T.S., et al. (2008). Reversal of blindness in animal models of leber congenital amaurosis using optimized AAV2-mediated gene transfer. Mol. Ther. *16*, 458–465.

11. Russell, S., Bennett, J., Wellman, J.A., Chung, D.C., Yu, Z.F., Tillman, A., Wittes, J., Pappas, J., Elci, O., McCague, S., et al. (2017). Efficacy and safety of voretigene neparvovec (AAV2-hRPE65v2) in patients with RPE65-mediated inherited retinal dystrophy: a randomised, controlled, open-label, phase 3 trial. Lancet *390*, 849–860.

12. Maguire, A.M., Simonelli, F., Pierce, E.A., Pugh, E.N., Jr., Mingozzi, F., Bennicelli, J., Banfi, S., Marshall, K.A., Testa, F., Surace, E.M., et al. (2008). Safety and efficacy of gene transfer for Leber's congenital amaurosis. N. Engl. J. Med. *358*, 2240–2248.

13. Bennett, J., Maguire, A.M., Cideciyan, A.V., Schnell, M., Glover, E., Anand, V., Aleman, T.S., Chirmule, N., Gupta, A.R., Huang, Y., et al. (1999). Stable transgene expression in rod photoreceptors after recombinant adeno-associated virus-mediated gene transfer to monkey retina. Proc. Natl. Acad. Sci. USA *96*, 9920–9925.

14. Bainbridge, J.W., Mehat, M.S., Sundaram, V., Robbie, S.J., Barker, S.E., Ripamonti, C., Georgiadis, A., Mowat, F.M., Beattie, S.G., Gardner, P.J., et al. (2015). Long-term effect of gene therapy on Leber's congenital amaurosis. N. Engl. J. Med. *372*, 87–1897.

15. Jacobson, S.G., Cideciyan, A.V., Roman, A.J., Sumaroka, A., Schwartz, S.B., Heon, E., and Hauswirth, W.W. (2015). Improvement and decline in vision with gene therapy in childhood blindness. N. Engl. J. Med. *372*, 1920–1926.

16. Anand, V., Maguire, A.M., and Bennett, J. (1999). High levels of transgene expression after readministration of adeno-associated virus to the subretinal space. Invest. Ophthalmol. Vis. Sci. *40*, S592.

17. Anand, V., Duffy, B., Yang, Z., Dejneka, N.S., Maguire, A.M., and Bennett, J. (2002). A deviant immune response to viral proteins and transgene product is generated on subretinal administration of adenovirus and adewno-associated virus. Mol. Ther. *5*, 125–132.

18. Jacobson, S.G., Acland, G.M., Aguirre, G.D., Aleman, T.S., Schwartz, S.B., Cideciyan, A.V., Zeiss, C.J., Komaromy, A.M., Kaushal, S., Roman, A.J., et al. (2006). Safety of recombinant adeno-associated virus type 2-RPE65 vector delivered by ocular subretinal injection. Mol. Ther. *13*, 1074–1084.

19. Bennett, J., Pakola, S., Zeng, Y., and Maguire, A. (1996). Humoral response after administration of E1-deleted adenoviruses: immune privilege of the subretinal space. Hum. Gene Ther. *7*, 1763–1769.

20. Bennett, J. (2003). Immune response following intraocular delivery of recombinant viral vectors. Gene Ther. *10*, 977–982.

21. Anand, V., Chirmule, N., Maguire, A.M., and Bennett, J. (2000). Induction of immune deviant response in the subretinal space is dependent on the nature of antigen introduced. IOVS *41*, S117.

22. Bennett, J., Wellman, J., Marshall, K.A., McCague, S., Ashtari, M., DiStefano-Pappas, J., Elci, O.U., Chung, D.C., Sun, J., Wright, J.F., et al. (2016). Safety and durability of effect of contralateral-eye administration of AAV2 gene therapy in patients with childhood-onset blindness caused by RPE65 mutations: a follow-on phase 1 trial. Lancet *388*, 661–672.

23. Bennett, J., Ashtari, M., Wellman, J., Marshall, K.A., Cyckowski, L.L., Chung, D.C., McCague, S., Pierce, E.A., Chen, Y., Bennicelli, J.L., et al. (2012). AAV2 gene therapy readministration in three adults with congenital blindness. Sci. Transl. Med. *4*, 120ra15.

24. Amado, D., Mingozzi, F., Hui, D., Bennicelli, J., Wei, Z., Chen, Y., et al. (2010). Safety and efficacy of subretinal re-administration of an AAV2 vector in large animal models: Implications for studies in humans. Sci. Transl. Med. *2*, 21ra16.

25. Annear, M.J., Bartoe, J.T., Barker, S.E., Smith, A.J., Curran, P.G., Bainbridge, J.W., Ali, R.R., and Petersen-Jones, S.M. (2011). Gene therapy in the second eye of RPE65-deficient dogs improves retinal function. Gene Ther. *18*, 53–61.

26. Chirmule, N., Propert, K., Magosin, S., Qian, Y., Qian, R., and Wilson, J. (1999). Immune responses to adenovirus and adeno-associated virus in humans. Gene Ther. *6*, 1574–1583.

27. Calcedo, R., and Wilson, J.M. (2016). AAV Natural Infection Induces Broad Cross-Neutralizing Antibody Responses to Multiple AAV Serotypes in Chimpanzees. Hum. Gene Ther. Clin. Dev. *27*, 79–82.

28. Curcio, C.A., Sloan, K.R., Jr., Packer, O., Hendrickson, A.E., and Kalina, R.E. (1987). Distribution of cones in human and monkey retina: individual variability and radial asymmetry. Science *236*, 579–582.

29. Bumsted, K., Jasoni, C., Szél, A., and Hendrickson, A. (1997). Spatial and temporal expression of cone opsins during monkey retinal development. J. Comp. Neurol. *378*, 117–134.

30. Bumsted, K., and Hendrickson, A. (1999). Distribution and development of short-wavelength cones differ between Macaca monkey and human fovea. J. Comp. Neurol. *403*, 502–516.

31. Jacobson, S.G., Boye, S.L., Aleman, T.S., Conlon, T.J., Zeiss, C.J., Roman, A.J., Cideciyan, A.V., Schwartz, S.B., Komaromy, A.M., Doobrajh, M., et al. (2006). Safety in nonhuman primates of ocular AAV2-RPE65, a candidate treatment for blindness in Leber congenital amaurosis. Hum. Gene Ther. *17*, 845–858.

32. Barreiro, L.B., Marioni, J.C., Blekhman, R., Stephens, M., and Gilad, Y. (2010). Functional comparison of innate immune signaling pathways in primates. PLoS Genet. *6*, e1001249.

33. Bjornson-Hooper, Z.B., Fragiadakis, G.K., Spitzer, M.H., Madhireddy, D., McIlwain, D., and Nolan, G.P. (2019). A comprehensive atlas of immunological differences between humans, mice and non-human primates. bioRxiv. https://doi.org/10.1101/574160.

34. Kennedy, C.J., Rakoczy, P.E., and Constable, I.J. (1995). Lipofuscin of the retinal pigment epithelium: a review. Eye (Lond.) *9*, 763–771.

35. Greenberg, J.P., Duncker, T., Woods, R.L., Smith, R.T., Sparrow, J.R., and Delori, F.C. (2013). Quantitative fundus autofluorescence in healthy eyes. Invest. Ophthalmol. Vis. Sci. *54*, 5684–5693.

36. Delori, F.C. (2004). Autofluorescence method to measure macular pigment optical densities fluorometry and autofluorescence imaging. Arch. Biochem. Biophys. *430*, 156–162.

37. Aleman, T., Tretiakova, A., Morgan, J., Lyubarsky, A., Zhou, E.E.W., et al. (2017). Safety of *RGX-314*, AAV8.

38. Katz, M.L., and Redmond, T.M. (2001). Effect of Rpe65 knockout on accumulation of lipofuscin fluorophores in the retinal pigment epithelium. Invest. Ophthalmol. Vis. Sci. *42*, 3023–3030.

39. Lorenz, B., Wabbels, B., Wegscheider, E., Hamel, C.P., Drexler, W., and Preising, M.N. (2004). Lack of fundus autofluorescence to 488 nanometers from childhood on in patients with early-onset severe retinal dystrophy associated with mutations in RPE65. Ophthalmology *111*, 1585–1594.

40. Lorenz, B., Poliakov, E., Schambeck, M., Friedburg, C., Preising, M.N., and Redmond, T.M. (2008). A comprehensive clinical and biochemical functional study of a novel RPE65 hypomorphic mutation. Invest. Ophthalmol. Vis. Sci. *49*, 5235–5242.

41. Perrin, G.Q., Herzog, R.W., and Markusic, D.M. (2019). Update on clinical gene therapy for hemophilia. Blood *133*, 407–414.

42. Peden, C.S., Manfredsson, F.P., Reimsnider, S.K., Poirier, A.E., Burger, C., Muzyczka, N., and Mandel, R.J. (2009). Striatal readministration of rAAV vectors reveals an immune response against AAV2 capsids that can be circumvented. Mol. Ther. *17*, 524–537.

43. Takahashi, K., Morizane, Y., Hisatomi, T., Tachibana, T., Kimura, S., Hosokawa, M.M., Shiode, Y., Hirano, M., Doi, S., Toshima, S., et al. (2018). The influence of subretinal injection pressure on the microstructure of the monkey retina. PLoS ONE *13*, e0209996.

44. Aleman, T.S., Cideciyan, A.V., Sumaroka, A., Schwartz, S.B., Roman, A.J., Windsor, E.A., Steinberg, J.D., Branham, K., Othman, M., Swaroop, A., and Jacobson, S.G. (2007). Inner retinal abnormalities in X-linked retinitis pigmentosa with RPGR mutations. Invest. Ophthalmol. Vis. Sci. *48*, 4759–4765.

45. Nti, A.A., Serrano, L.W., Sandhu, H.S., Uyhazi, K.E., Edelstein, I.D., Zhou, E.J., et al. (2018). Frequent subclinical macular changes in combined BRAF/MEKinhibition with high-dose hydroxychloroquine as treatment for advanced BRAF mutant melanoma: Preliminary results from a phase I/II clinical treatment trial. Retina *39*, 502–513.

46. Simonett, J.M., Grewal, D.S., Fawzi, A.A., Lyon, A.T., and Gill, M.K. (2016). Fundus Autofluorescence Patterns of Submacular Fluid Resolution Following Repair of Macula-Involving Rhegmatogenous Retinal Detachments. Ophthalmic Surg. Lasers Imaging Retina *47*, 1020–1029.

47. Nork, T.M., Murphy, C.J., Kim, C.B., Ver Hoeve, J.N., Rasmussen, C.A., Miller, P.E., Wabers, H.D., Neider, M.W., Dubielzig, R.R., McCulloh, R.J., and Christian, B.J. (2012). Functional and anatomic consequences of subretinal dosing in the cynomolgus macaque. Arch. Ophthalmol. *130*, 65–75.

48. Reichel, F.F., Dauletbekov, D.L., Klein, R., Peters, T., Ochakovski, G.A., Seitz, I.P., Wilhelm, B., Ueffing, M., Biel, M., Wissinger, B., et al. (2017). AAV8 Can Induce Innate and Adaptive Immune Response in the Primate Eye. Mol Ther. *25*, 2648–2660.

49. Peters, T., Seitz, I.P., Michalakis, S., Biel, M., Wilhelm, B., Reichel, F.F., et al. (2019). Safety and toxicology of ocular gene therapy with recombinant AAV Vector rAAV.hCNGA3 in non-human primates. Hum. Gene Ther. Clin. Dev.

50. Marmor, M.F., Yao, X.Y., and Hageman, G.S. (1994). Retinal adhesiveness in surgically enucleated human eyes. Retina *14*, 181–186.

51. Szurman, P., Roters, S., Grisanti, S., Aisenbrey, S., Schraermeyer, U., Lüke, M., Bartz-Schmidt, K.U., and Thumann, G. (2006). Ultrastructural changes after artificial retinal detachment with modified retinal adhesion. Invest. Ophthalmol. Vis. Sci. *47*, 4983–4989.

52. Xue, K., Groppe, M., Salvetti, A.P., and MacLaren, R.E. (2017). Technique of retinal gene therapy: delivery of viral vector into the subretinal space. Eye (Lond.) *31*, 1308–1316.

53. You, Y.S., Lee, C.Y., Li, C., Lee, S.H., Kim, K., and Jung, H. (2014). An arched microinjector (ARCMI) for innocuous subretinal injection. PLoS ONE *9*, e104145.

54. Fischer, M.D., Hickey, D.G., Singh, M.S., and MacLaren, R.E. (2016). Evaluation of an Optimized Injection System for Retinal Gene Therapy in Human Patients. Hum. Gene Ther. Methods *27*, 150–158.

55. Ochakovski, G.A., Peters, T., Michalakis, S., Wilhelm, B., Wissinger, B., Biel, M., Bartz-Schmidt, K.U., and Fischer, M.D.; RD-CURE Consortium (2017). Subretinal Injection for Gene Therapy Does Not Cause Clinically Significant Outer Nuclear Layer Thinning in Normal Primate Foveae. Invest. Ophthalmol. Vis. Sci. *58*, 4155–4160.

56. Seitz, I.P., Michalakis, S., Wilhelm, B., Reichel, F.F., Ochakovski, G.A., Zrenner, E., Ueffing, M., Biel, M., Wissinger, B., Bartz-Schmidt, K.U., et al.; RD-CURE Consortium (2017). Superior Retinal Gene Transfer and Biodistribution Profile of Subretinal Versus Intravitreal Delivery of AAV8 in Nonhuman Primates. Invest. Ophthalmol. Vis. Sci. *58*, 5792–5801.

57. Rakoczy, E.P., Lai, C.M., Magno, A.L., Wikstrom, M.E., French, M.A., Pierce, C.M., Schwartz, S.D., Blumenkranz, M.S., Chalberg, T.W., Degli-Esposti, M.A., and Constable, I.J. (2015). Gene therapy with recombinant adeno-associated vectors for neovascular age-related macular degeneration: 1 year follow-up of a phase 1 randomised clinical trial. Lancet *386*, 2395–2403.

58. Qiao-Grider, Y., Hung, L.F., Kee, C.S., Ramamirtham, R., and Smith, E.L., 3rd (2007). Normal ocular development in young rhesus monkeys (Macaca mulatta). Vision Res. *47*, 1424–1444.

59. Maguire, A.M., High, K.A., Auricchio, A., Wright, J.F., Pierce, E.A., Testa, F., Mingozzi, F., Bennicelli, J.L., Ying, G.S., Rossi, S., et al. (2009). Age-dependent effects of RPE65 gene therapy for Leber's congenital amaurosis: a phase 1 dose-escalation trial. Lancet *374*, 1597–1605.

60. Aleman, T.S., Uyhazi, K.E., Serrano, L.W., Vasireddy, V., Bowman, S.J., Ammar, M.J., Pearson, D.J., Maguire, A.M., and Bennett, J. (2018). RDH12 Mutations Cause a Severe Retinal Degeneration With Relatively Spared Rod Function. Invest. Ophthalmol. Vis. Sci. *59*, 5225–5236.

OMTM, Volume *15*

Supplemental Information

Safety of Same-Eye Subretinal Sequential Readministration of *AAV2-hRPE65v2* in Non-human Primates

Lindsey Weed, Michael J. Ammar, Shangzhen Zhou, Zhangyong Wei, Leona W. Serrano, Junwei Sun, Vivian Lee, Albert M. Maguire, Jean Bennett, and Tomas S. Aleman

Supplementary Figures

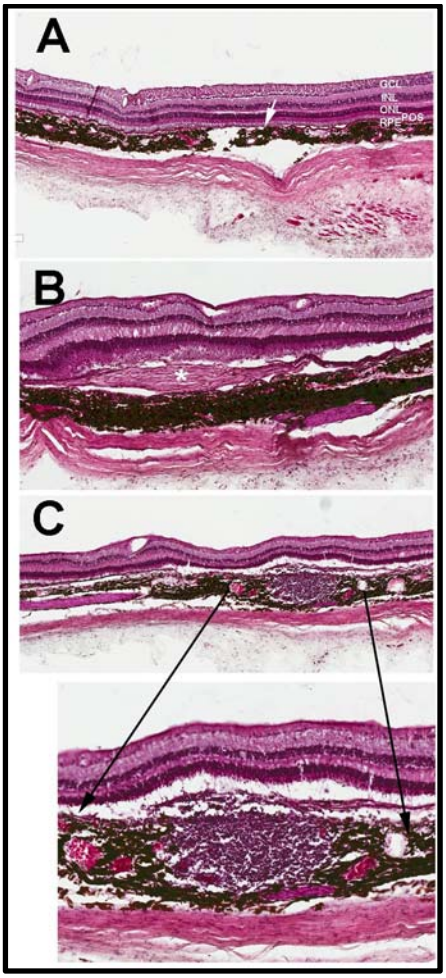

Fig. S1. Examples of focal and rare histopathologic findings. Shown are hematoxylin and eosin-stained cryosections from the right retina of 11D086. (A) There is a focal break in the RPE layer (arrow) coinciding with shortening of outer segments. B) Fibrinoid scar (*) is present in the subretinal space; (C) focal collection of monocytes in the choroid, extending towards subretinal space. The RPE is missing in this area. Inset shows a higher magnification view of this area. GCL, ganglion cell layer; INL, inner nuclear layer; ONL, outer nuclear layer; POS, photoreceptor outer segment; RPE, retinal pigmented epithelium.

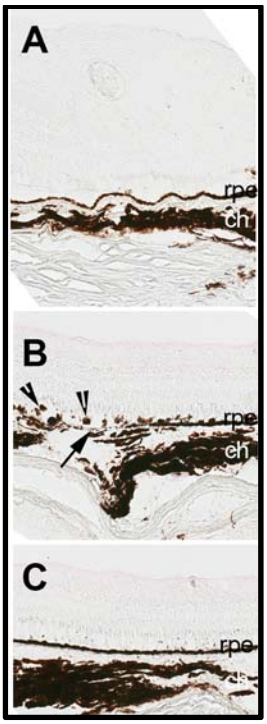

Fig. S2. Representative RPE65 immunohistochemistry results after ipsilateral subretinal readministration in a non-human primate (BF54F) in (A) injection region #1, (B) overlapping injection region, and (C) on injection region #2. (B) Arrowheads, dislodged RPE cells; arrow, atrophic retinal pigmented epithelium (RPE) cells; ch, choroid

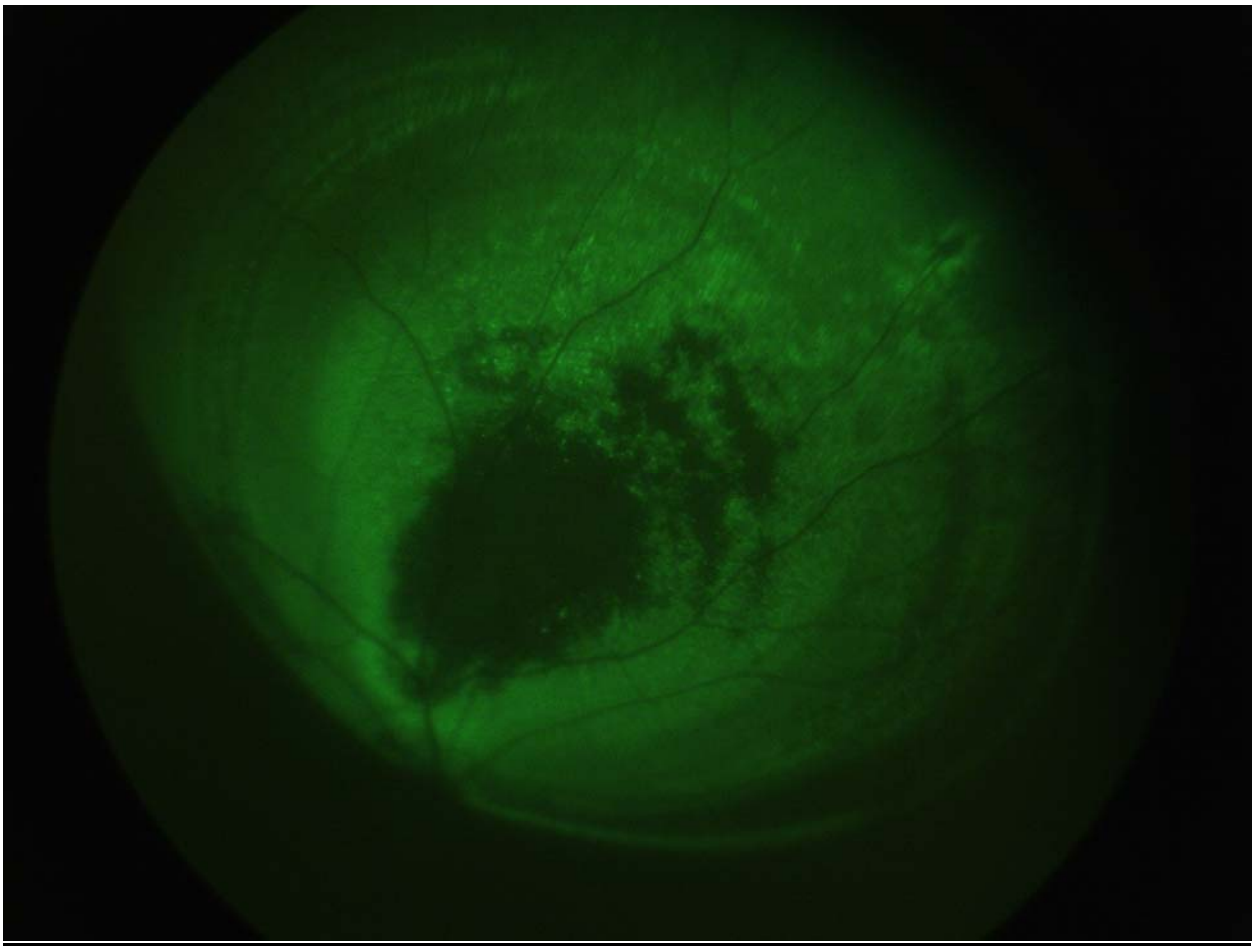

Fig. S3. Example of contour map-like appearance effect documented by imaging with a RetCam equipped with fluorescein filters after subretinal injection of AAV.EGFP in a NHP. This animal had received a subretinal injection of 1E11vg of a tyrosine-mutant AAV (AAV2TYF) carrying CVM-driven enhanced green fluorescent protein (EGFP) three months earlier. The image shows EGFP fluorescence occupying the region exposed to the AAV. A ringlike pattern is detected surrounding a black-appearing center of the bleb.